Study of Circumferential Waves on a Poroelastic Cylinder

Jan Descheemaeker, Christ Glorieux, Walter Lauriks, Jean-Philippe Groby, Philippe Leclaire, Laurens Boeckx

Study of Circumferential Waves on a Poroelastic Cylinder

J. Descheemaeker[1)], C. Glorieux[1)], W. Lauriks[1)], J. P. Groby[2)], P. Leclaire[3)], L. Boeckx[4)]

[1)] Laborature Acoustical and Thermal Fysica, Katholieke Universiteit Leuven, Celestijnenlaan 200D, 3001 Heverlee, Belgium. jan.descheemaeker@fys.kuleuven.be

[2)] Laboratoire d'Acoustique de l'Université du Maine, UMR CNRS 6613, Avenue Olivier Messiaen, 72085 Le Mans Cedex 9, France.

[3)] Institut Supérieur de l'Automobile et des Transports - Université de Bourgogne, 49 Rue Mademoiselle Bourgeois, 58027 Nevers Cedex, France.

[4)] Huntsman Europe, Everslaan 45, 3078 Everberg, Belgium.

Summary

The dispersion relations of acoustic modes in poroelastic cylinders with and without elastic shell coating are determined and solved. The influence of elastic frame parameters and the Biot parameters on the dispersion curves is studied in the configuration with and without coating. The dispersive Rayleigh and whispering gallery waves are highly sensitive to the density and the shear modulus of the skeleton, opening a perspective for the evaluation of the mechanical parameters of poroelastic materials confined in cylindrical tubes during the manufacturing process. The predicted dispersion curves are validated with experimental results obtained by use of different experimental set-up in the case of a porous circular cylinder.

PACS no. 43.20.Jr

1. Introduction

The determination of the effective acoustic parameters of sound absorbing porous materials has received quite some attention during the last decades. However, both in low and ultrasonic frequency ranges, the issue of accurately determining the elastic parameters needs further attention. The difficulty lies in the fact that frame materials are often viscoelastic, i.e. the Lamé coefficients are frequency dependent. Traditional quasi-static or vibrational techniques enable the recovery of these elastic parameters [1, 2, 3, 4] in the low frequency range (up to 500 Hz–1 kHz), but there is a need for extension of the accessible frequency range. Recently[5, 6], the frequency dependence of the elastic parameters of the frame of a poroelastic material was determined in the kHz range from the analysis of the wave propagation in a poroelastic semi-infinite half space (Rayleigh wave), in a poroelastic plate (Lamb waves) and in a poroelastic plate on a rigid surface (Lamb-like waves).

Poroelastic materials are typically confined in a cylindrical holder during the process of their manufacturing and testing. The monitoring of the poroelastic parameters while the material is changing from a liquid mixture to a solid foam during the polymerization process, as well as the evaluation of the final elastic modulus of the foam materials is of considerable interest for foam manufacturers. The phase velocities of the waves associated with modes are also studied when the porous cylinder is coated with an elastic shell. The latter simulates the container in which the polymerisation stands. This article is a first step toward the determination of the variation of the elastic properties, mainly the shear modulus and the density of the frame, during the manufacturing process of the porous sample. During the liquid phase, the cells are closed and the foam behaves as a visco-elastic material. At the end of the process, the cells are open and the foam behaves as a poroelastic material. The manufacturer knows when the foam has raised and we will monitor the rising of the foam at the end of the process.

With this goal, the approach in [5, 6] is further explored, and extended to a cylindrical geometry. Rayleigh waves in elastic cylinders[7] or in a coated elastic cylinder[8] were extensively studied. To our knowledge, the present study is the first one that deals with Rayleigh waves in poroelastic cylinders.

Contrary to its homologue in a semi-infinite half space, in circular shape configurations, the Rayleigh wave, which corresponds to the lowest velocity mode as evaluated from the dispersion relations, is dispersive. The effect of dispersion is particularly visible at low frequencies, where the wavelength becomes of the order of the radius. The high frequency limit of the velocity dispersion curve tends to the Rayleigh velocity of the material in a semi-infinite half-space. Note that this dispersion is geometric and it should be distinguished from the material dispersion, e.g.

due to porosity. While the dispersive Rayleigh wave propagates along the surface of the cylinder, the energy of whispering gallery waves, which travel at higher velocities, and exist due to the curvature of the surface, is more concentrated in the inner part of the cylinder[9]. Whispering gallery waves can be represented in a ray model as the result of multiple reflections around the inner surface of the cylinder. Below a cut-off frequency they are highly damped.

Cylindrical porous materials were already studied in geophysics. Schmitt studied the process of drilling holes, which modifies the physical properties of the formation close to the borewall, leading to different coaxial, saturated porous shells [10].

In section 2, the calculation model that enables the determination and solution of the dispersion relation for waves in a (coated) poroelastic cylinder is briefly described. Dispersion curves are simulated, and the possible extraction of the poroelastic modulus from the phase velocity measurements is evaluated. Results of a sensitivity analysis, in which the dependence is determined of the wave velocity, in particular for the dispersive Rayleigh wave, on the shear modulus and the density of the frame, are presented in section 3. Also the influence of the elastic coating is investigated. Finally, the results of experiments performed by two techniques on a poroelastic circular cylinder are presented and compared with the theoretical predictions.

2. Waves in a circular porous cylinder with and without elastic coating

As an extension of the study of circumferential waves in layered elastic cylinders [11], in this section we numerically determine the frequency dependence of the phase velocities of whispering gallery waves and of the dispersive Rayleigh wave in a porous cylinder with and without an elastic shell coating. For every frequency, the velocities of different modes are found by searching the roots of a characteristic determinant, which is obtained by combining the wave equations with the boundary conditions that characterize the geometrical configuration, in the absence of a source.

After projection on an appropriate basis and assuming sinusoidal solutions, most of the acoustic problems are reduced to the solution of a linear system of the form $\mathbf{D}\cdot\mathbf{U}=\mathbf{S}$, where $\mathbf{U}$ is the unknown vector, $\mathbf{D}$ is the propagation matrix and $\mathbf{S}$ the solicitation vector. In the absence of a driving source, $\mathbf{S}=\mathbf{0}$, non-trivial solutions (the so called modes), are obtained when $\det(\mathbf{D})=0$. The roots of this determinant, which contains the material properties and is a function of the wavenumber and frequency of the modes, then lead to the relation between the phase velocity and frequency (c,ω) of the modes. In the particular case of circular cylindrical geometry, these roots are pairs (n,ω) and the projection on the basis explicitly provides a propagation matrix that depends on n, the order of the Hankel and Bessel functions involved.

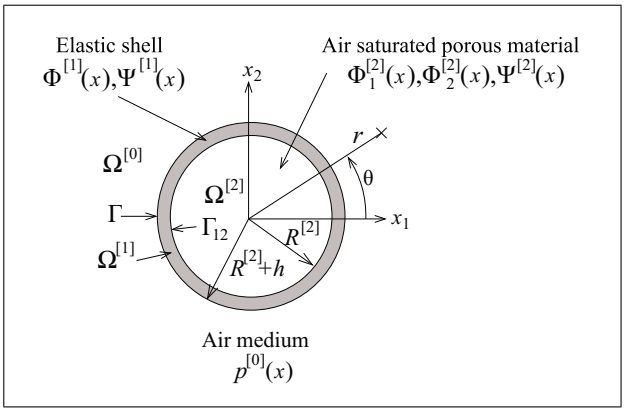

Figure 1. Cross-sectional plane view of the configuration of a poroelastic cylinder coated with an elastic shell.

2.1. Description of the configuration

The geometrical configuration is assumed to be invariant with respect to the Cartesian coordinate x_3.

Figure 1 depicts a cross-sectional plane view of the configuration. The domain $\Omega^{[0]}$ represents the fluid medium around the porous cylinder $M^{[0]}$. A polar coordinate system (r,O,θ) is used to, with its origin in the center of the cylinder ($\Omega^{[2]}$) of radius $R^{[2]}$ filled with poroelastic material $M^{[2]}$ saturated by the fluid $M^{[0]}$. The cylinder is either in welded contact with the domain $\Omega^{[0]}$ through the interface Γ, or in welded contact with an elastic coating $M^{[1]}$, occupying the domain $\Omega^{[1]}$ of thickness h through the interface Γ_{12}. In the case of a coated cylinder, $\Omega^{[1]}$ is in welded contact with $\Omega^{[0]}$ through the interface Γ at $R^{[2]}+h$. The radius of Γ will be denoted by $R^{[0]}$ for both configurations.

2.2. Field representations and material modeling

Rather than to solve directly for $\bar{\mathbf{a}}(\mathbf{x},t)$, $\bar{\mathbf{a}}(\mathbf{x},t)$ being either a vector or a scalar possibly denoting the time dependent pressure, displacement, scalar or vector potentials, etc., the following analysis is done for sinusoidal solutions. In the frequency domain we work with the Fourier transform, $\mathbf{a}(\mathbf{x},\omega)$, related to $\bar{\mathbf{a}}(\mathbf{x},t)$ through $\bar{\mathbf{a}}(\mathbf{x},t)=\int_{-\infty}^{\infty}\mathbf{a}(\mathbf{x},\omega)\mathrm{e}^{-\mathrm{i}\omega t}d\omega$. Henceforth, we also drop the ω dependence in $\mathbf{a}(\mathbf{x},\omega)$, so as to denote the latter $\mathbf{a}(\mathbf{x})$.

In $\Omega^{[0]}$, the scattered pressure field can be written as

$$p^{[0]}(\mathbf{x})=\sum_{n\in\mathbb{Z}}B_n\mathrm{H}_n^{(1)}\left(k^{[0]}r\right)\mathrm{e}^{\mathrm{i}n\theta}, \tag{1}$$

wherein $\mathrm{H}_n^{(1)}$ is the n-th order Hankel function of first kind, $k^{[0]}$ is the wavenumber in $\Omega^{[0]}$, and B_n are the scattered coefficients by the circular cylinder.

When an elastic coating is considered, the scattered scalar $\phi^{[1]}$ and vector $\boldsymbol{\psi}^{[1]}=\psi^{[1]}\mathbf{i}_3$ potentials in $\Omega^{[1]}$, related to the displacement $\mathbf{u}^{[1]}$ through $\mathbf{u}^{[1]}=\nabla\phi^{[1]}+\nabla\times\boldsymbol{\psi}^{[1]}$ take the forms

$$\begin{aligned}\phi^{[1]}(\mathbf{x}) &= \sum_{n\in\mathbb{Z}}\left[C_n\mathrm{J}_n\left(k_P^{[1]}r\right)+D_n\mathrm{H}_n^{(1)}\left(k_P^{[1]}r\right)\right]\mathrm{e}^{\mathrm{i}n\theta},\\ \psi^{[1]}(\mathbf{x}) &= \sum_{n\in\mathbb{Z}}\left[E_n\mathrm{J}_n\left(k_S^{[1]}r\right)+F_n\mathrm{H}_n^{(1)}\left(k_S^{[1]}r\right)\right]\mathrm{e}^{\mathrm{i}n\theta},\end{aligned} \tag{2}$$

wherein J_n is the n-th order Bessel function, $k_P^{[1]} = \omega/c_P^{[1]}$ and $k_S^{[1]} = \omega/c_S^{[1]}$ are the wave numbers associated with compressional and shear waves, and C_n, D_n, E_n and F_n the coefficients of the diffracted potentials in $\Omega^{[1]}$. The constitutive equation in $\Omega^{[1]}$ can be written in the form

$$\begin{aligned}\sigma_{ij}(\mathbf{x}) &= \lambda^{[1]} e_{mm}\delta_{ij} + 2\mu^{[1]} e_{ij} \\ &= -\lambda^{[1]}\left(k_P^{[1]}\right)^2 \phi^{[1]}\delta_{ij} + 2\mu^{[1]} e_{ij},\end{aligned} \tag{3}$$

wherein the Einstein summation is implicit, δ_{ij} is the Kronecker delta, $\boldsymbol{\sigma}$ the stress tensor, $\mathbf{e} = \left(\nabla\mathbf{u}^{[1]} + \nabla^T\mathbf{u}^{[1]}\right)/2$ the strain tensor, and $\lambda^{[1]}$ and $\mu^{[1]}$ are the Lamé coefficients of $M^{[1]}$.

In $\Omega^{[2]}$, the scattered scalar $\phi_1^{[2]}$ and $\phi_2^{[2]}$ and vector $\boldsymbol{\psi}^{[2]} = \psi^{[2]}\mathbf{i}_3$ potentials, related to the displacements $\mathbf{u}^{[2]}$ in the solid phase through $\mathbf{u}^{[2]} = \nabla(\phi_1^{[2]}+\phi_2^{[2]}) + \nabla\times\boldsymbol{\psi}^{[2]} = \nabla\phi^{[2s]} + \nabla\times\boldsymbol{\psi}^{[2]}$ and $\mathbf{U}^{[2]}$ in the fluid phase through $\mathbf{U}^{[2]} = \nabla(\mu_1\phi_1^{[2]} + \mu_2\phi_2^{[2]}) + \nabla\times\mu_3\boldsymbol{\psi}^{[2]} = \nabla\phi^{[2f]} + \nabla\times\mu_3\boldsymbol{\psi}^{[2]}$ take the forms

$$\begin{aligned}\phi_1^{[2]}(\mathbf{x}) &= \sum_{n\in\mathbb{Z}} G_n \mathrm{J}_n\left(k_1^{[2]}r\right)\mathrm{e}^{\mathrm{i}n\theta}, \\ \phi_2^{[2]}(\mathbf{x}) &= \sum_{n\in\mathbb{Z}} M_n \mathrm{J}_n\left(k_2^{[2]}r\right)\mathrm{e}^{\mathrm{i}n\theta}, \\ \psi^{[2]}(\mathbf{x}) &= \sum_{n\in\mathbb{Z}} O_n \mathrm{J}_n\left(k_3^{[2]}r\right)\mathrm{e}^{\mathrm{i}n\theta},\end{aligned} \tag{4}$$

wherein $k_i^{[2]}$ (i=1, 2, 3) are the wave numbers associated respectively with the so-called fast, slow and shear waves, and G_n, M_n, and O_n are the coefficients of the diffracted potentials inside the cylinder. The expressions of μ_i and $k_i^{[2]}$ (i=1, 2, 3) can be found in[12]. The constitutive relations in $\Omega^{[2]}$ read as

$$\begin{aligned}\sigma_{ij}^s(\mathbf{x}) &= \left[(P-2N)\,e_{mm} + Q\varepsilon_{mm}\right]\delta_{ij} + 2Ne_{ij} \\ &= a_1\left(k_1^{[2]}\right)^2\phi_1^{[2]} + a_2\left(k_2^{[2]}\right)^2\phi_2^{[2]} + 2Ne_{ij}, \\ \sigma_{ij}^f(\mathbf{x}) &= \left[Qe_{mm} + R\varepsilon_{mm}\right]\delta_{ij} \\ &= -b_1\left(k_1^{[2]}\right)^2\phi_1^{[2]} - b_2\left(k_2^{[2]}\right)^2\phi_2^{[2]} = \phi p^{[2]},\end{aligned} \tag{5}$$

wherein $a_i = 2N - P - Q\mu_i$ and $b_i = Q + R\mu_i$, $i = 1, 2$, and $\boldsymbol{\varepsilon} = \left(\nabla U^{[2]} + \nabla^T U^{[2]}\right)/2$. The expressions of R, Q, and P are[12]

$$\begin{aligned}R &= \phi K_f, \\ Q &= \frac{R(1-\phi)}{\phi}, \\ P &= \frac{(1-\phi)\left((1-\phi) - K_{sm}/K_s\right)K_s + \phi K_s/K_f K_{sm}}{(1-\phi) - K_{sm}/K_s + \phi K_s/K_f} \\ &\quad + (4/3)N,\end{aligned} \tag{6}$$

where K_f is the compressibility of the saturating fluid, which is in considered to be identical to the ambient fluid, i.e. the air medium. K_{sm} and $K_s = K_{sm}/(1-\phi(Q+R)/R)$ are respectively the compressibility of the frame and of the solid material, N is the shear modulus and ϕ the porosity. Young's modulus E and Poisson's ratio ν, related to N, and K_{sm} through $N = E/2(1+\nu)$, $K_{sm} = EN/(3(3N-3))$ are used as an alternative to E and N.

The thermal and viscous losses are accounted for by use of the Johnson-Champoux-Allard model [13, 14], which involves the tortuosity α_∞, the viscous (Λ) and thermal (Λ') characteristic lengths and the flow resistivity σ.

2.3. Circular poroelastic cylinder saturated by air

Since $M^{[0]}$ is a fluid medium and $M^{[2]}$ is a poroelastic material, the normal total stress, pressure and normal component of the displacement should be continuous across Γ,

$$\begin{cases}\sigma_{rr}^s(R^{[0]},\theta) + \sigma_{rr}^f(R^{[0]},\theta) + p^{[0]}(R^{[0]},\theta) = 0, \\ \sigma_{r\theta}^s(R^{[0]},\theta) = 0, \\ -\sigma_{rr}^f(R^{[0]},\theta)/\phi - p^{[0]}(R^{[0]},\theta)) = 0, \\ u_r^{[2]}(R^{[0]},\theta) + w_r^{[2]}(R^{[0]},\theta) - U_r^{[0]}(R^{[0]},\theta) = 0,\end{cases} \tag{7}$$

wherein $\mathbf{w}^{[2]} = \phi(\mathbf{U}^{[2]} - \mathbf{u}^{[2]})$ is the relative solid-fluid displacement[15].

Introducing the proper field and potential expressions, equations (1) and (4), in equation (7), projecting the latter on the appropriate basis, i.e. $\int_0^{2\pi}\cdot\times\mathrm{e}^{-\mathrm{i}l\theta}\,\mathrm{d}\theta$ and making use of the orthogonality relation $\int_0^{2\pi}\cdot\times\mathrm{e}^{\mathrm{i}(n-l)\theta} = 2\pi\delta_{ln}$, lead, after rearrangement, to a propagation matrix

$$\mathbf{D} = \begin{bmatrix} a_{11} & a_{12} & \cdots & a_{13} & \left(R^{[0]}\right)^2\mathrm{H}_n^{(1)}\left(\alpha^{[0]}\right) \\ a_{21}/N & a_{22}/N & & a_{23}/N & 0 \\ a_{31}d_1 & a_{32}d_2 & & a_{33}d_2 & -\alpha^{[0]}\dot{\mathrm{H}}_n^{(1)}\left(\alpha^{[0]}\right)/\left(k^{[0]}\right)^2K^{[0]} \\ b_1\left(\alpha_1^{[2]}\right)^2\mathrm{J}_n\left(\alpha_1^{[2]}\right) & b_2\left(\alpha_2^{[2]}\right)^2\mathrm{J}_n\left(\alpha_2^{[2]}\right) & & 0 & -\left(R^{[0]}\right)^2\phi\mathrm{H}_n^{(1)}\left(\alpha^{[0]}\right) \end{bmatrix} \tag{8}$$

with the unknown column vector $\mathbf{U} = \langle G_n,\ M_n,\ O_n,\ B_n\rangle$ formed by the diffraction coefficients of each domain involved in the configuration. In (8), $d_i = 1 + \phi(\mu_i - 1)$, $i = 1, 2$, $\alpha_i^{[j]} = k_i^{[j]}R^{[0]}$, $i = 1, 2$ and $j = 0, 2$, and $K^{[0]}$ the compressibility of $M^{[0]}$ are introduced. The expression of the matrix elements are reported in Appendix 5.

2.4. Circular poroelastic cylinder saturated by air and coated with an elastic material

Since $M^{[0]}$ is a fluid medium and $M^{[1]}$ is an elastic material, the normal stress and normal component of the displacement should be continuous across Γ,

$$\begin{cases}\sigma_{rr}^{[1]}(R^{[0]},\theta) + p^{[0]}(R^{[0]},\theta) = 0, \\ \sigma_{r\theta}^{[1]}(R^{[0]},\theta) = 0, \\ u_r^{[1]}(R^{[0]},\theta) - U_r^{[0]}(R^{[0]},\theta) = 0.\end{cases} \tag{9}$$

Since $M^{[1]}$ is an elastic material and $M^{[2]}$ is a poroelastic material, the normal total stress and the displacements should be continuous across Γ_{12},

$$\begin{cases}\sigma_{rr}^s(R^{[2]},\theta) + \sigma_{rr}^f(R^{[2]},\theta) - \sigma_{rr}^{[1]}(R^{[2]},\theta) = 0, \\ \sigma_{r\theta}^s(R^{[2]},\theta) - \sigma_{r\theta}^{[1]}(R^{[2]},\theta) = 0, \\ u_r^{[2]}(R^{[2]},\theta) - u_r^{[1]}(R^{[2]},\theta) = 0, \\ u_\theta^{[2]}(R^{[2]},\theta) - u_\theta^{[1]}(R^{[2]},\theta) = 0, \\ u_r^{[2]}(R^{[2]},\theta) - U_r^{[2]}(R^{[2]},\theta) = 0.\end{cases} \tag{10}$$

Proceeding as in section 2.3, the propagation matrix becomes

$$\mathbf{D} = \begin{bmatrix} a_{11} & a_{12} & a_{13} & a_{14} & a_{15} & a_{16} & a_{17} & 0 \\ a_{21} & a_{22} & a_{23} & a_{24} & a_{25} & a_{26} & a_{27} & 0 \\ a_{31} & a_{32} & a_{33} & a_{34} & a_{35} & a_{36} & a_{37} & 0 \\ 0 & 0 & 0 & a_{44} & a_{45} & a_{46} & a_{47} & a_{48} \\ 0 & 0 & 0 & a_{54} & 0 & a_{56} & a_{57} & 0 \\ 0 & 0 & 0 & a_{64} & 0 & a_{66} & a_{67} & a_{68} \\ a_{71} & a_{72} & a_{73} & 0 & a_{75} & a_{76} & a_{77} & a_{78} \\ a_{81} & a_{82} & a_{83} & 0 & 0 & 0 & 0 & 0 \end{bmatrix} \quad (11)$$

with the unknown column vector

$$\mathbf{U} = \left\langle G_n,\ M_n,\ O_n,\ B_n,\ C_n,\ D_n,\ E_n,\ F_n \right\rangle$$

formed by the diffraction coefficients of each domain involved in the configuration and the expression of the matrix elements given in the Appendix 5.

2.5. Numerical evaluation of the roots of the dispersion curves

The determinant of $\mathbf{D}(n, \omega)$ was calculated as a function of frequency $\omega = 2\pi f$ and of the order of the Bessel and Hankel functions n. The pairs (ω_{min}, n_{min}) for which $|\det(\mathbf{D}(n, \omega))|$ is minimum typically correspond with the zeros of the determinant. The phase velocity v of the corresponding modes can then be evaluated as $v = \omega_{min} R / n_{min}$ in the case of a poroelastic cylinder, and as $v = \omega_{min}(R + h/2)(1 + \frac{h}{2(R+h/2)})/n_{min}$ in the case of a porous cylinder covered by an elastic coating[8].

For non dissipative materials, the minima of $|\det(\mathbf{D})|$ correspond to the roots of $\det(\mathbf{D}) = 0$ because these roots are real, with the exception of leaky modes. For dissipative materials, such as poroelastic foams, the roots of $\det(\mathbf{D}) = 0$ are complex. Considering a dissipative material as a perturbation of a non-dissipative one, dissipation can be accounted for by introducing complex shear modulus and phase velocities. As a result, the roots of $\det(\mathbf{D}) = 0$ are then shifted from the real axis in the complex plane. A classical way to solve the dispersion equation would imply looking for a complex order of Bessel and Hankel funstions n. However, evaluating these functions is not straightforward and the involved calculation time makes this approach rather cumbersome. Most of the available routines enable the evaluation of Bessel and Hankel functions of integer or real order, but none of them enable their evaluation for complex order. For this reason, we have chosen to approximate the real part of the phase velocity by using the expressions above with pairs (ω_{min}, n_{min}) that minimize $|\det(\mathbf{D})|$.

3. Numerical results and discussion

As a typical poroelastic material, we have chosen for the current study the material Fireflex (Recticel, Wetteren, Belgium). Values of the parameters of this material were determined by traditional methods [16, 17] and are summarized in Table I. The radius of the cylinder was $R^{[2]} = 75$ mm. The Rayleigh wave velocity of this material in a plane, semi-infinite configuration c_R is 38 m/s. This value was determined by means of the method described in [5, 17].

Table I. Parameters of the Fireflex (Recticel, Wetteren, Belgium), i.e. the poroelastic material studied in this paper.

ϕ	α_∞	σ (Ns/m^4)	Λ (μm)
0.95	1.42	8900	180
Λ' (μm)	N (Pa)	E (Pa)	ρ (kg/m^3)
360	56000	140000	32

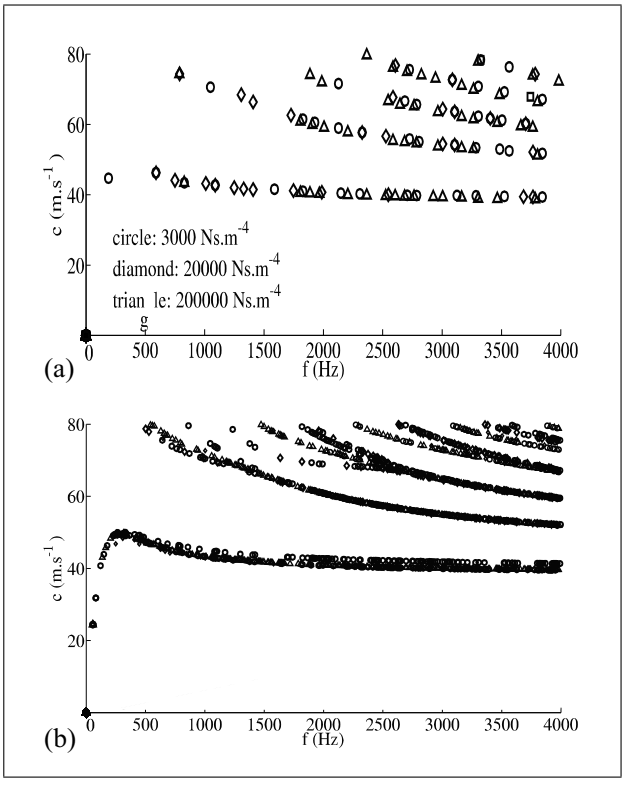

Figure 2. Phase velocity c of the Rayleigh and of the whispering gallery waves as calculated for a Fireflex cylinder (material parameters: Table I) (—). The symbols represent curves obtained for one of the parameters varied, the other ones kept fixed: (a) sensitivity to the flow resistivity ($\sigma = 3000$Ns.m^{-4} (o), $\sigma = 20000$Ns.m^{-4} ($\diamond$), and $\sigma = 200000$Ns.m^{-4} ($\triangle$)), (b) sensitivity to the porosity: ($\phi = 0$ (o), $\phi = 0.3$ ($\triangle$), $\phi = 0.95$ ($\square$)).

3.1. Numerical results for porous cylinder saturated by air

The frequency dependence of the phase velocity of dispersive Rayleigh and whispering gallery waves, as calculated with the help of the previously described method, is shown in Figure 2. Below 1500 Hz, the geometric dispersion of the dispersive Rayleigh wave is clearly noticeable, and at high frequencies the velocity tends to ≈ 40 m/s, in correspondence with the value for c_R mentioned above.

In the following, we address the influence of the Biot parameters on the phase velocities of the waves associated

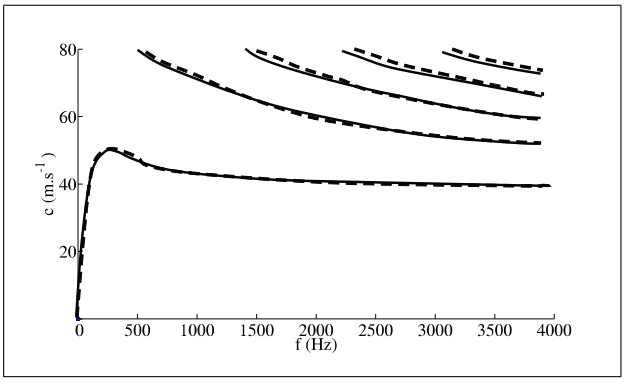

Figure 3. Simulation with a porous cylinder of Fireflex (—) and visco-elastic cylinder with density equal to the density of the frame material (– – –).

with the modes. One by one, parameters are varied, while keeping the other parameters fixed.

The dispersion curves turn out to be quasi insensitive to variations of the flow resistivity between 3000 Ns.m^{-4} and 200000 Ns.m^{-4} (Figure 2a). This is not surprising, since the energy of these waves, particularly the dispersive Rayleigh wave, is mainly carried by the skeleton. The sensitivity of the dispersion curves on the porosity is shown in Figure 2. Only for porosities smaller than 30%, a small effect of maximum 4% occurs in the phase velocity of the modes. The lower order modes of the poroelastic Fireflex cylinder are approximated very well by the ones of a (virtual) non-porous visco-elastic cylinder with the same elastic parameters and with density taken equal to the density of the frame, as shown in Figure 3. There is a little difference for higher order modes around their cut-off frequency. The fact that the differences are small is due to the fact that the material is highly porous and the air-solid interaction is weak. The theory with a porous layer is more general and is worth studying as it would apply to low porosity materials or materials saturated by a heavier fluid.

Figure 4 shows that the dispersion curves are strongly sensitive to variations of the shear modulus (a) as well as to variations of the density (b) of the frame, and only weakly sensitive to the longitudinal modulus of the frame, in accordance with [6] for horizontal geometries. Figure 4a shows that when the shear modulus is decreased with 50%, the Rayleigh velocity decreases from 165 m/s to 50 m/s. Figure 4b shows that when the density is decreased by a factor 70%, the Rayleigh velocity increases from 22 m/s to 42 m/s.

It is well known that the high frequency limit of the Rayleigh wave velocity is mainly determined by the shear velocity, which, for viscoelastic materials, is equal to the square root of the ratio of the shear modulus and the density. As a result, quite often effects on the dispersion curves due to changes in shear modulus can be compensated by changes in density. Figure 5 shows that indeed the effect of shear modulus and density on the dispersion curves is highly degenerate: when the shear modulus and density are simultaneously doubled, then in the case of a porous cylinder of Fireflex without coating, then the dispersion curves

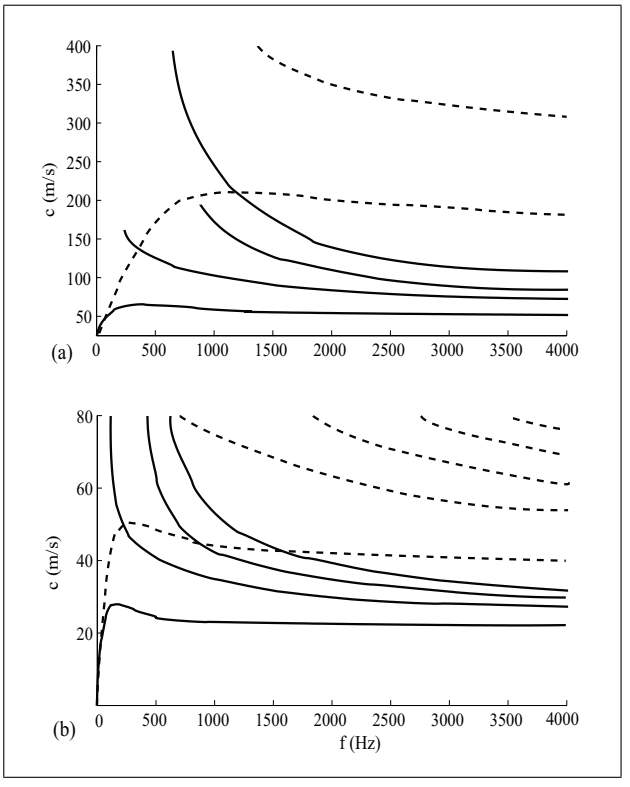

Figure 4. Sensitivity of the phase velocity of the dispersive Rayleigh and of the lowest three whispering gallery waves as calculated for a Fireflex-material-like cylinder: (a) variation of the shear modulus: $N = 10^5$ Pa, ρ =32 kg/m^3 (– – –) and $N = 5 \times 10^4$ Pa, ρ =32 kg/m^3 (—) and (b) variation of the density: ρ =30 kg/m^3, $N = 56000$ Pa (– – –) and ρ =100 kg/m^3, $N = 56000$ Pa (—).

remain unchanged. For the coated cylinder, there is a minor difference at low frequencies. This degeneracy is not problematic, since for most applications alternative techniques can be used to determine the density. The guided acoustic wave method can then be used to determine the shear modulus only, using an a priori determined value for the density. The high sensitivity of the considered waves to the value of the shear modulus opens nice perspectives to use this parameter as an indicator during the transition between the fluid to the solid phase while a foam is rising.

3.2. Numerical simulations for a porous cylinder with an elastic coating

We have performed a similar analysis for a coated foam cylinder, which is encountered quite frequently in manufacturing situations. Due to the presence of the elastic coating, it can be expected that the sensitivity is deteriorated due to the coating layer being typically stiffer than the foam of interest, thus dominating the Rayleigh wave propagation characteristics. However, for sufficiently low frequencies, the waves are expected to penetrate deeply into the foam, thus becoming sensitive to its properties.

Two coatings were considered with $h = 1$ mm thickness, one made up of poly(methyl metacrylate) (PMMA) ($c_P^{[1]} = 2740$ m/s, $c_S^{[1]} = 1120$ m/s and $\rho^{[1]} = 1180$ kg/m^3)

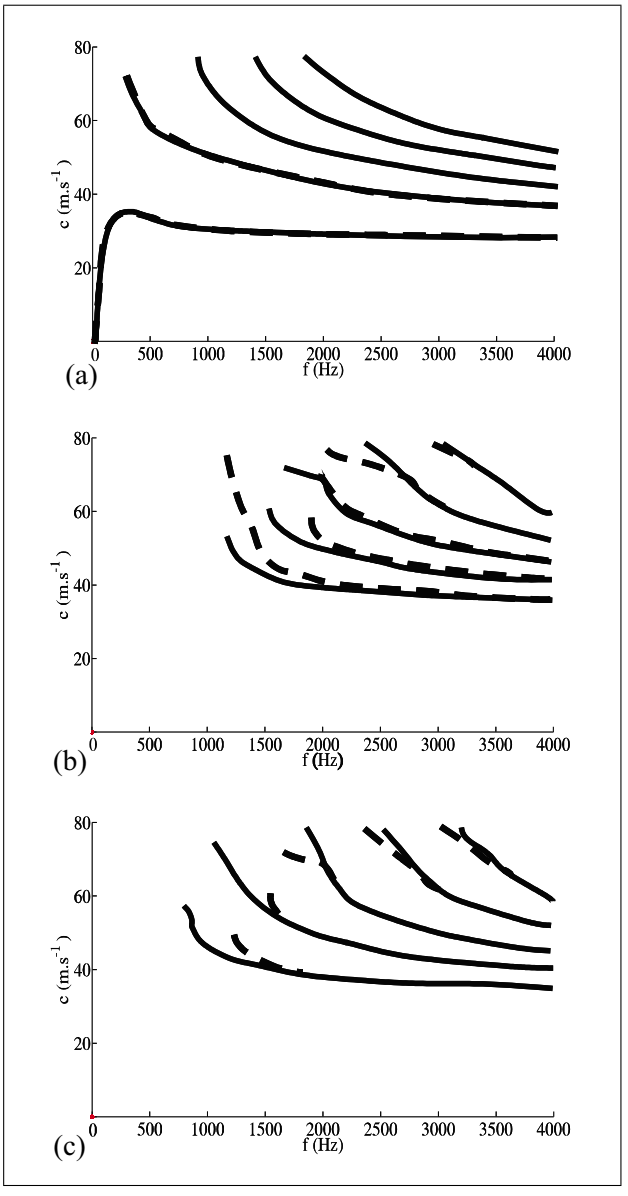

Figure 5. Dispersion curves for a Fireflex cylinder without coating (a), a Fireflex cylinder with PMMA coating (b) and a Fireflex cylinder with steel coating (c). The shear modulus and density are multiplied with the same factor: $N = 25000$ Pa and density 16 kg.m^{-3} (—), $N = 50000$ Pa and density 32 kg.m^{-3} (− − −).

and one of steel ($c_P^{[1]} = 6320$ m/s, $c_S^{[1]} = 3230$ m/s and $\rho^{[1]} = 7700$ kg/m^3). Simulations were performed for a poroelastic cylinder of Fireflex with a shear modulus of $N = 5 \times 10^4$ Pa and $N = 1 \times 10^5$ Pa, Figure 6. Due to the coating, the wave mode that tends at high frequencies to the Rayleigh wave velocity of the bulk material disappears. However, higher order wave modes still exist. Since these modes are becoming faster with increasing shear modulus of the foam, it can be concluded that they can be associated with modified whispering gallery waves of the foam, and also that analyzing the dispersion of these modes allows to elastically characterize the foam. The possibility for characterizing the foam is thus not affected by the presence of a steel or PMMA coating. The proposed method to determine or monitor the foam density and shear modulus thus remains effective when the foam is contained in a cylindrical tube e.g. during the polymerization process.

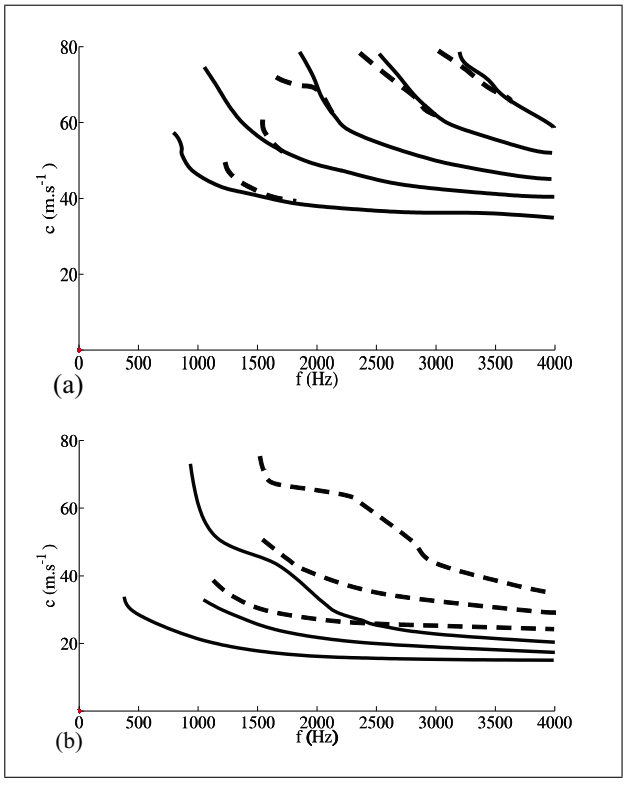

Figure 6. Phase velocity of the lowest three modes of a Fireflex cylinder of $N = 10000$ Pa, ρ =32 kg/m^3 (− − −) and of $N = 50000$ Pa, ρ =32 kg/m^3 (—): (a) coated with PMMA and (b) coated with steel.

4. Experimental validation

4.1. Experimental methods

Two experimental methods were used to determine the dispersion curves of the modes propagating in the system.

A schematic overview of the experimental setup used to determine the dispersion curves of the modes propagating in the system is depicted Figure 7. Using a shaker (Q-sources), circumferential waves were generated on the surface of a porous sample. The normal component of the surface velocity was detected by a Laser Vibrometer (Polytec OFV-505), at different distances from the generation site. A cylindrical Fireflex sample of radius 7.5 cm was placed centered on a circular rotating plate. The shaker was firmly attached to the sample so that there was no relative motion between them. It was fairly small and light and could provide signals at frequencies up to 10 kHz. The distance between the source and the detection point could be varied by rotating the set shaker/sample, while keeping the laser beam unchanged. The rotation angle of the sample was precision controlled by means of a cable connecting the periphery of the circular disk to a computer controlled linear translation stage (a linear stepping motor).

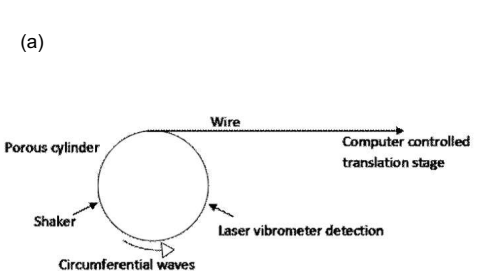

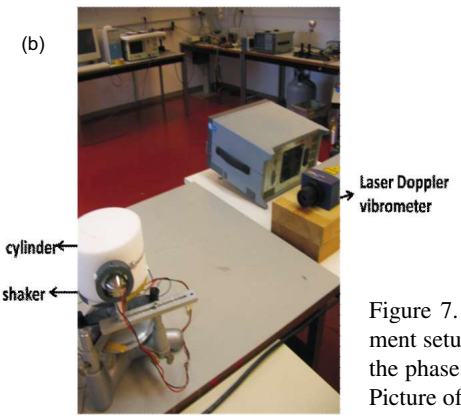

Figure 7. a) Schematical measurement setup for the determination of the phase velocity of the modes. b) Picture of the measurement setup.

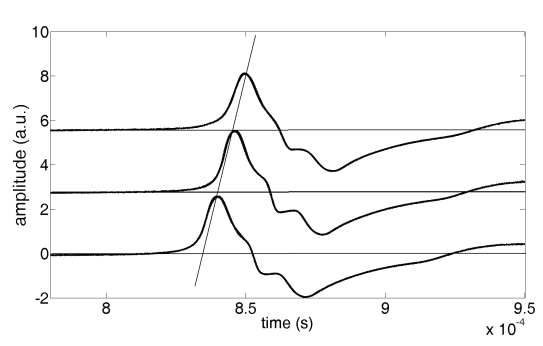

Figure 8. Example of 3 waveforms propagating along the surface of a poroelastic cylinder in the case of pulse excitation. The signals were detected at different distances from the source in steps of $\Delta x = 0.028$ mm. The curves are plotted with an off-set for clarity.

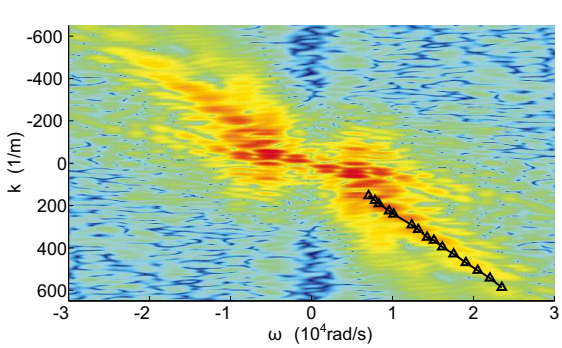

Figure 9. Example of dispersion curves from $|S(k,\omega)|$ for a Fireflex cylinder. The line is a mode of the Fireflex cylinder that can be detected. The triangles are the experimental data extracted from the result in in Figure 12.

A narrow strip of steel, with dimensions 0.5 cm × 3 cm, was glued to the shaker, thus acting as a line source generating circumferential waves along the surface of the cylindrical sample. The strip was oriented parallel to the axis of the cylinder. A strip of reflecting tape with negligible thickness was glued tangentially on the surface of the cylinder so that the circumferential waves could be detected by the vibrometer at different angular positions along the surface.

4.1.1. Pulse excitation

In a first configuration, transient waves were excited by means of a pulser-receiver (Panametrics model 5058 PR) sending a short pulse (with a length of 10^{-4} s and a height of 2.5 V) to the shaker. Figure 8 shows some waveforms detected at different distances from the generation site. The diagonal line clearly shows the time shift of the signal. The distance between two pulses is $\Delta x = 0.028$ mm.

This configuration is a variant of the one used in [6]. In this method, by recording the signals on a digital oscilloscope (Lecroy 9310M) at regularly spaced distances from the excitation source, a two-dimensional signal matrix $S(x,t)$ is acquired. By appropriately choosing the resolution in time and in space, dispersion curves can be directly obtained by taking the dual time and space Fourier Transform, thus providing the 2D spectrum $S(k,\omega)$.

The maximum curves in the 2D map of $|S(k,\omega)|$ correspond with the dispersion curves $k(\omega)$ of respective wave modes. Figure 9 shows an example of an experimentally obtained dispersion curve, from which the phase velocities of the modes could be determined by $c = \omega/k$. The key advantage of this technique is that it simultaneously provides the dispersion curves of several modes, even if the velocities of the modes are close to each other.

4.1.2. Sine burst excitation

In a second configuration, a function generator provided a rather narrowband sinusoidal burst (with duration of $20T$, with $T = 1/f$ the sinusoidal period and f the frequency) to the shaker. Also in this method the waves can be detected by a laser Doppler vibrometer and recorded by an oscilloscope. The phase velocity of a wave can be determined by determining the differences in arrival time of the waves collected at several distances ($\Delta x = 2$ mm) from the source, cfr Figure 10.

The slope of the curve, which was obtained by plotting the recording distances Δx as a function of the arrival times Δt, was used to determine the phase velocity using

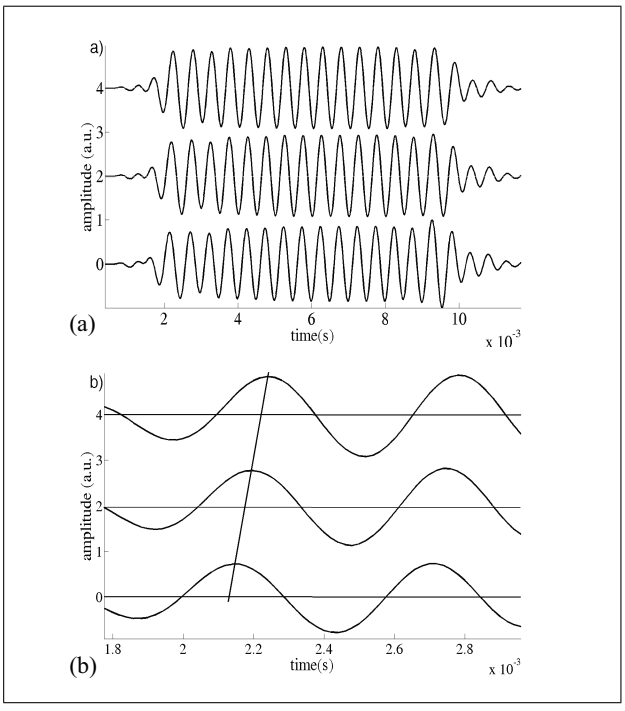

Figure 10. Example of a) response to sine bursts detected at various distances from the source (the steplength Δx is 2 mm) and b) zoom on the time difference between the maxima. The curves are plotted with an off-set for clarity.

the relation $2\pi\Delta t/T = \Delta\phi = -k\Delta x = -(\omega/c(\omega))\Delta x$. These arrival times were estimated by cross correlating the signal at different locations with the one obtained on the detection position closest to the source (Figure 10). An example of a linear fit performed to determine the phase velocity is plotted Figure 11. This method provides a better signal to noise ratio than the pulse method, which is expected to be very valuable for highly damping poroelastic foams. However, the method is not applicable when modes have very similar velocities, since in that case the respective waveforms are hard to distinguish in time domain ([5]).

4.2. Experimental results

Experimental dispersion curves as obtained with the pulse excitation method (△) and with the burst excitation method (□) are compared in Figure 12 for the Fireflex poroelastic cylinder under investigation. The experimental data are compared with simulated dispersion curves calculated on the basis of the literature values listed in Table I. In the analyzed frequency range, the dispersion curves match quite well. Due to the large damping and thus rather short accessible distance range, it was difficult to accurately extract data at lower wave numbers and frequencies. Both experimental methods enable the evaluation of the dispersive Rayleigh wave for frequencies between 1 kHz and 4 kHz. For higher frequencies, the burst method cannot be used, due to the proximity of several modes in velocity and thus in arrival time of the respective bursts, which results in overlapping.

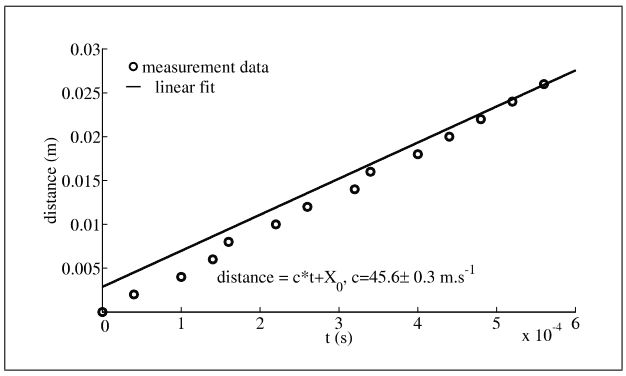

Figure 11. Example of a distance (to the first measurement point) versus time curve for the determination of the phase velocity.

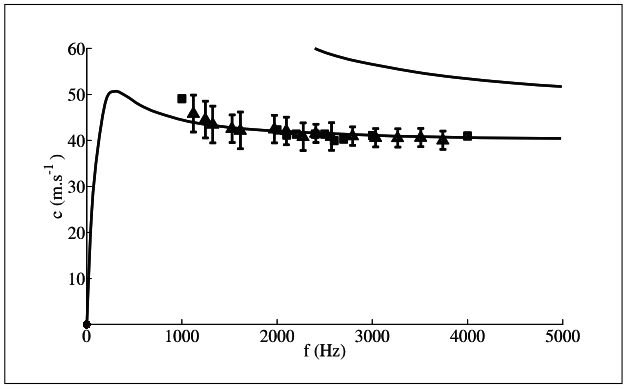

Figure 12. Experimental (△ pulse excitation and □ burst excitation) and theoretical (—) phase velocities for a Fireflex cylinder.

In the asymptotic high frequency regime, both the theory and experiments tend to a Rayleigh velocity around 40 m/s.

4.3. Extraction of the frequency dependence of the shear modulus

The simulations above have shown that both the shear modulus and density significantly influence the phase velocities, while the other parameters only weakly affect the dispersion curves.

Since the density can be determined simply by other methods and since its influence is degenerated with the influence of the shear modulus, here we focus on the experimental extraction of the shear modulus. This is done by performing a one-parameter minimization of a cost function involving the available experimental data for the lowest order mode.

The common way to recover the shear modulus would be to minimize the sum of squared differencies between the measured velocities and the calculated velocities. This procedure requires the highly time consuming evaluation of the root(s) of the determinant at each iteration. Here, we follow an alternative approach. Given that the dispersion curves are found by minimizing $F = |\det(D(\omega, v, N))|$, and that the experimental value for v_{exp} for every given ω_{exp} is known, N, the parameter of interest, can be found for every frequency by minimizing the function $F(N)$ for

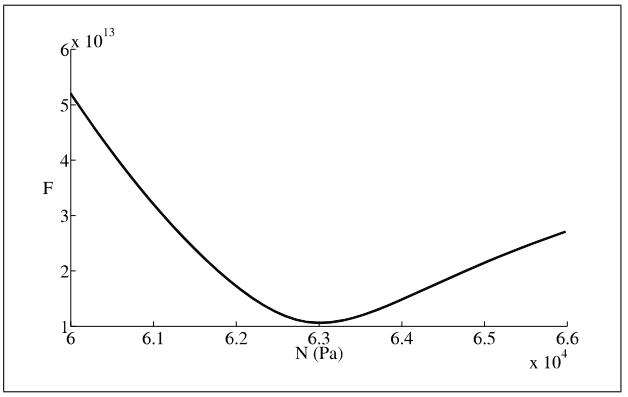

Figure 13. Evolution of F as a function of the shear modulus. The minimum corresponds to the extracted shear modulus.

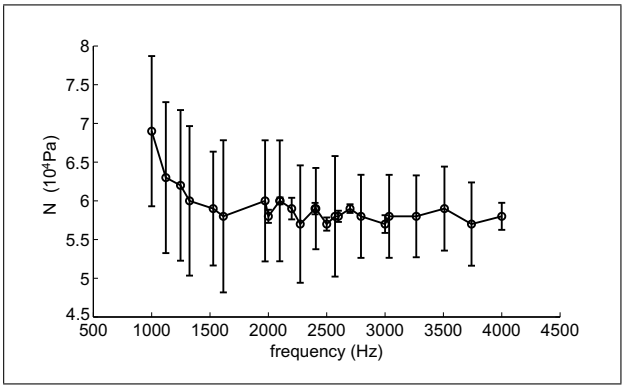

Figure 14. Shear moduli found with a numerical inversion of the experimental results of Figure 12.

that frequency and corresponding experimental velocity. An example of this procedure is illustrated in Figure 14 for $f = 1.1\,kHz$.

The shear moduli found with this numerical inversion method (Figure 14) are roughly frequency independent and correspond reasonably well with the literature value of Table I.

5. Conclusion

A theoretical model was developed for the numerical evaluation of the phase velocities of modes in the configuration of a poroelastic cylinder with and without elastic coating. Simulations were made with a porous cylinder of Fireflex and an elastic coating of steel and PMMA. The influence of the Biot parameters of the poroelastic material on the dispersion curves of the modes was studied. Acoustic and structural parameters, i.e. the porosity, the tortuosity, the thermal and viscous characteristic lengths and flow resistivity were found to have no or small influence on the phase velocities of the dispersive Rayleigh and whispering gallery waves. On the other hand, the shear modulus and density of the foam skeleton do have a large and rather degenerate influence on the phase velocities of the modes, both for a bare cylinder and for a cylinder coated with an elastic shell. Hence the phase velocity determination in (coated) cylindrical sample configurations gives a suitable way to experimentally determine and industrially monitor the shear modulus of poroelastic foams during the production process.

Both burst excitation and pulse excitation were used to determine the phase velocities of the waves propagating along the surface of a Fireflex porous cylinder with and without coating. Good agreement was found between the experimental results and the numerical simulations between 1 kHz and 4 kHz.

Appendix

Expression of the elements of the driving agent matrices

The matrix elements in the determinant of the boundary conditions from section 2.4 for a porous cylinder with (without) an elastic coating are

$$
\begin{aligned}
a_{11} &= \left(\bar{\alpha}_1^{[2]}\right)^2\left((a_1-b_1)\mathrm{J}_n\left(\bar{\alpha}_1^{[2]}\right)+2N\ddot{\mathrm{J}}_n\left(\bar{\alpha}_1^{[2]}\right)\right)\\
a_{12} &= \left(\bar{\alpha}_2^{[2]}\right)^2\left((a_2-b_2)\mathrm{J}_n\left(\bar{\alpha}_2^{[2]}\right)+2N\ddot{\mathrm{J}}_n\left(\bar{\alpha}_2^{[2]}\right)\right)\\
a_{13} &= 2Nin\left(\bar{\alpha}_3^{[2]}\dot{\mathrm{J}}_n\left(\bar{\alpha}_3^{[2]}\right)-\mathrm{J}_n\left(\bar{\alpha}_3^{[2]}\right)\right)\\
a_{14} &= -\left(\bar{\alpha}_P^{[1]}\right)^2\left(-\lambda^{[1]}\mathrm{J}_n\left(\bar{\alpha}_P^{[1]}\right)+2\mu^{[1]}\ddot{\mathrm{J}}_n\left(\bar{\alpha}_P^{[1]}\right)\right)\\
a_{15} &= -\left(\bar{\alpha}_P^{[1]}\right)^2\Big(-\lambda^{[1]}\mathrm{H}_n^{(1)}\left(\bar{\alpha}_P^{[1]}\right)\\
&\qquad +2\mu^{[1]}\ddot{\mathrm{H}}_n^{(1)}\left(\bar{\alpha}_P^{[1]}\right)\Big)\\
a_{16} &= -2\mu^{[1]}in\left(\bar{\alpha}_S^{[1]}\dot{\mathrm{J}}_n\left(\bar{\alpha}_S^{[1]}\right)-\mathrm{J}_n\left(\bar{\alpha}_S^{[1]}\right)\right)\\
a_{17} &= -2\mu^{[1]}in\left(\bar{\alpha}_S^{[1]}\dot{\mathrm{H}}_n^{(1)}\left(\bar{\alpha}_S^{[1]}\right)-\mathrm{H}_n^{(1)}\left(\bar{\alpha}_S^{[1]}\right)\right)
\end{aligned}
\tag{A1}
$$

$$
\begin{aligned}
a_{21} &= 2Nin\left(\bar{\alpha}_1^{[2]}\dot{\mathrm{J}}_n\left(\bar{\alpha}_1^{[2]}\right)-\mathrm{J}_n\left(\bar{\alpha}_1^{[2]}\right)\right)\\
a_{22} &= 2Nin\left(\bar{\alpha}_2^{[2]}\dot{\mathrm{J}}_n\left(\bar{\alpha}_2^{[2]}\right)-\mathrm{J}_n\left(\bar{\alpha}_2^{[2]}\right)\right)\\
a_{23} &= N\Big(-\left(\bar{\alpha}_3^{[2]}\right)^2\ddot{\mathrm{J}}_n\left(\bar{\alpha}_3^{[2]}\right)+\bar{\alpha}_3^{[2]}\dot{\mathrm{J}}_n\left(\bar{\alpha}_3^{[2]}\right)\\
&\qquad -n^2\mathrm{J}_n\left(\bar{\alpha}_3^{[2]}\right)\Big)\\
a_{24} &= 2\mu^{(1)}in\left(\bar{\alpha}_P^{[1]}\dot{\mathrm{J}}_n\left(\bar{\alpha}_P^{[1]}\right)-\mathrm{J}_n\left(\bar{\alpha}_P^{[1]}\right)\right)\\
a_{25} &= 2\mu^{(1)}in\left(\bar{\alpha}_P^{[1]}\dot{\mathrm{H}}_n^{(1)}\left(\bar{\alpha}_P^{[1]}\right)-\mathrm{H}_n(1)\left(\bar{\alpha}_P^{[1]}\right)\right)\\
a_{26} &= \mu^{(1)}\Big(\left(\bar{\alpha}_S^{[1]}\right)^2\ddot{\mathrm{J}}_n\left(\bar{\alpha}_S^{[1]}\right)-\bar{\alpha}_S^{[1]}\dot{\mathrm{J}}_n\left(\bar{\alpha}_S^{[1]}\right)\\
&\qquad +n^2\mathrm{J}_n\left(\bar{\alpha}_S^{[1]}\right)\Big)\\
a_{27} &= \mu^{(1)}\Big(\left(\bar{\alpha}_S^{[1]}\right)^2\ddot{\mathrm{H}}_n^{(1)}\left(\bar{\alpha}_S^{[1]}\right)-\bar{\alpha}_S^{[1]}\dot{\mathrm{H}}_n^{(1)}\left(\bar{\alpha}_S^{[1]}\right)\\
&\qquad +n^2\mathrm{H}_n^{(1)}\left(\bar{\alpha}_S^{[1]}\right)\Big)
\end{aligned}
\tag{A2}
$$

$$
\begin{aligned}
a_{31} &= \bar{\alpha}_1^{[2]}\dot{\mathrm{J}}_n\left(\bar{\alpha}_1^{[2]}\right)\\
a_{32} &= \bar{\alpha}_2^{[2]}\dot{\mathrm{J}}_n\left(\bar{\alpha}_2^{[2]}\right)\\
a_{33} &= in\mathrm{J}_n\left(\bar{\alpha}_3^{[2]}\right)\\
a_{34} &= -\bar{\alpha}_P^{[1]}\dot{\mathrm{J}}_n\left(\bar{\alpha}_P^{[1]}\right)\\
a_{35} &= -\bar{\alpha}_P^{[1]}\dot{\mathrm{H}}_n^{(1)}\left(\bar{\alpha}_P^{[1]}\right)\\
a_{36} &= -in\mathrm{J}_n\left(\bar{\alpha}_S^{[1]}\right)\\
a_{37} &= -in\mathrm{H}_n\left(\bar{\alpha}_S^{[1]}\right)
\end{aligned}
\tag{A3}
$$

$$
\begin{aligned}
a_{44} &= \left(\alpha_P^{[1]}\right)^2\left(-\lambda^{[1]}\mathrm{J}_n\left(\alpha_P^{[1]}\right)+2\mu^{[1]}\ddot{\mathrm{J}}_n\left(\alpha_P^{[1]}\right)\right)\\
a_{45} &= \left(\alpha_P^{[1]}\right)^2\left(-\lambda^{[1]}\mathrm{H}_n^{(1)}\left(\alpha_P^{[1]}\right)+2\mu^{[1]}\ddot{\mathrm{H}}_n^{(1)}\left(\alpha_P^{[1]}\right)\right)\\
a_{46} &= 2\mu^{[1]}in\left(\alpha_S^{[1]}\dot{\mathrm{J}}_n\left(\alpha_S^{[1]}\right)-\mathrm{J}_n\left(\alpha_S^{[1]}\right)\right)
\end{aligned}
\tag{A4}
$$

$$
\begin{aligned}
a_{47} &= 2\mu^{[1]}\mathrm{i}n\left(\alpha_S^{[1]}\dot{\mathrm{H}}_n^{(1)}\left(\alpha_S^{[1]}\right) - \mathrm{H}_n^{(1)}\left(\alpha_S^{[1]}\right)\right)\\
a_{48} &= \left(R^{[0]}\right)^2\mathrm{H}_n^{(1)}\left(\alpha^{[0]}\right)
\end{aligned}
$$

$$
\begin{aligned}
a_{54} &= 2\mathrm{i}n\left(\alpha_P^{[1]}\dot{\mathrm{J}}_n\left(\alpha_P^{[1]}\right) - \mathrm{J}_n\left(\alpha_P^{[1]}\right)\right)\\
a_{55} &= 2\mathrm{i}n\left(\alpha_P^{[1]}\dot{\mathrm{H}}_n^{(1)}\left(\alpha_P^{[1]}\right) - \mathrm{H}_n(1)\left(\alpha_P^{[1]}\right)\right)\\
a_{56} &= -\left(\alpha_S^{[1]}\right)^2\ddot{\mathrm{J}}_n\left(\alpha_S^{[1]}\right) + \alpha_S^{[1]}\dot{\mathrm{J}}_n\left(\alpha_S^{[1]}\right) - n^2\mathrm{J}_n\left(\alpha_S^{[1]}\right)\\
a_{57} &= -\left(\alpha_S^{[1]}\right)^2\ddot{\mathrm{H}}_n^{(1)}\left(\alpha_S^{[1]}\right) + \alpha_S^{[1]}\dot{\mathrm{H}}_n^{(1)}\left(\alpha_S^{[1]}\right)\\
&\quad -n^2\mathrm{H}_n^{(1)}\left(\alpha_S^{[1]}\right)
\end{aligned}
\tag{A5}
$$

$$
\begin{aligned}
a_{64} &= \alpha_P^{[1]}\dot{\mathrm{J}}_n\left(\alpha_P^{[1]}\right)\\
a_{65} &= \alpha_P^{[1]}\dot{\mathrm{H}}_n^{(1)}\left(\alpha_P^{[1]}\right)\\
a_{66} &= \mathrm{i}n\mathrm{J}_n\left(\alpha_S^{[1]}\right)\\
a_{67} &= \mathrm{i}n\mathrm{H}_n^{(1)}\left(\alpha_S^{[1]}\right)\\
a_{68} &= -\frac{\alpha^{[0]}}{\left(k^{[0]}\right)^2K^{[0]}}\dot{\mathrm{H}}_n^{(1)}\left(\alpha^{[0]}\right)
\end{aligned}
\tag{A6}
$$

$$
\begin{aligned}
a_{71} &= \mathrm{i}n\mathrm{J}_n\left(\bar{\alpha}_1^{[2]}\right)\\
a_{72} &= \mathrm{i}n\mathrm{J}_n\left(\bar{\alpha}_2^{[2]}\right)\\
a_{73} &= -\bar{\alpha}_3^{[2]}\dot{\mathrm{J}}_n\left(\bar{\alpha}_3^{[2]}\right)\\
a_{74} &= -\mathrm{i}n\mathrm{J}_n\left(\bar{\alpha}_P^{[1]}\right)\\
a_{75} &= -\mathrm{i}n\mathrm{H}_n\left(\bar{\alpha}_P^{[1]}\right)\\
a_{76} &= \bar{\alpha}_S^{[1]}\dot{\mathrm{J}}_n\left(\bar{\alpha}_S^{[1]}\right)\\
a_{77} &= \bar{\alpha}_S^{[1]}\dot{\mathrm{H}}_n^{(1)}\left(\bar{\alpha}_S^{[1]}\right)
\end{aligned}
\tag{A7}
$$

$$
\begin{aligned}
a_{81} &= \left(\mu_1 - 1\right)\bar{\alpha}_1^{[2]}\dot{\mathrm{J}}_n\left(\bar{\alpha}_1^{[2]}\right)\\
a_{82} &= \left(\mu_2 - 1\right)\bar{\alpha}_2^{[2]}\dot{\mathrm{J}}_n\left(\bar{\alpha}_2^{[2]}\right)\\
a_{83} &= \left(\mu_3 - 1\right)\mathrm{i}n\mathrm{J}_n\left(\bar{\alpha}_3^{[2]}\right)
\end{aligned}
\tag{A8}
$$

with $\alpha_j^{[1]} = k_j^{[1]}R^{[0]}$, $\bar{\alpha}_j^{[1]} = k_j^{[1]}R^{[2]}$, $j = P$ *(compressional)*, S *(shear)*, and $\bar{\alpha}_i^{[2]} = k_i^{[2]}R^{[2]}$, $i = 1, 2, 3$.

Acknowledgement

The authors would like to thank the Research Council of the K. U. Leuven for financial support provided by Project No. OT/07/035

References

[1] T. Pritz: Transfer function method for investigating the complex modulus of acoustic materials: spring-like method. J. Sound Vib. **72** (1980) 317–341.

[2] T. Pritz: Transfer function method for investigating the complex modulus of acoustic materials: rod-like method. J. Sound Vib. **81** (1982) 359–376.

[3] P. Leclaire: The vibrational response of a clamped rectangular porous plate. J. Sound Vib. **247** (2001) 19–31.

[4] M. Etchessahar, S. Sahraoui, L. Benyahia, J. F. Tassin: Frequency depencence of elastic properties of acoustic foams. J. Acoust. Soc. Am. **117** (2005) 1114–1121.

[5] L. Boeckx, P. Leclaire, P. Khurana, C. Glorieux, W. Lauriks, J. F. Allard: Investigation of the phase velocities of guided acoustic waves in soft porous layers. J. Acoust. Soc. Am. **117** (2005) 545–554.

[6] L. Boeckx, P. Leclaire, P. Khurana, C. Glorieux, W. Lauriks, J. F. Allard: Guided elastic waves in porous materials saturated by air under lamb conditions. J. Appl. Phys. **97** (2005) 094911.

[7] D. Clorennec, D. Royer: Analysis of surface acoustic wave propagation on a cylinder using laser ultrasonics. Appl. Phys. Lett. **82** (2003) 4608–4610.

[8] U. Kawald, C. Desmet, W. Lauriks, C. Glorieux, J. Thoen: Investigation of the dispersion relations of surface acoustic waves propagating on a layered cylinder. J. Acoust. Soc. Am. **99** (1996) 926–930.

[9] D. Royer, D. Clorennec: Theoretical and experimental investigation of rayleigh waves on cylindrical and spherical surfaces. 1st International Symposium on Laser Ultrasonics: Science, Technology and ApplicationsS (L.U. 2008), Montreal, Canada, 2008.

[10] D. P. Schmitt: Effects of radial layering when logging in saturated porous formations. J. Acoust. Soc. Am. **84** (1988) 2200–2214.

[11] C. Valle, J. Qu, L. J. Jacobs: Guided circumferential waves in layered cylinders. International Journal of Engeneering Science **37** (1999) 1369–138.

[12] M. A. Biot, D. G. Willis: The elastic coeffecients of the theory of consolidation. J. Appl. Mechanics **24** (1957) 594–601.

[13] D. J. Johnson, J. Koplik, R. Dashen: Theory of dynamic permeability and tortuosity in fluid-saturated porous media. J. Fluid Mech. **176** (1987) 379–402.

[14] J.-F. Allard, Y. Champoux: New empirical equations for sound propagation in rigid frame porous materials. J. Acoust. Soc. Am. **91** (1992) 3346–3353.

[15] T. Bourbie, O. Coussy, B. Zinszner: Acoustics of porous media. Technip, Paris, 1987.

[16] J.-F. Allard, N. Atalla: Propagation of sound in porous media: Modelling sound absorbing materials. Wiley, Chichester, 2009.

[17] J. F. Allard, G. Jansens, G. Vermeir, W. Walter: Frame borne surface waves in air-saturated porous media. J. Acoust. Soc. Am. **111** (2001) 690–696.